

NEUROTECHNOLOGY

A regenerative peripheral nerve interface allows real-time control of an artificial hand in upper limb amputees

Philip P. Vu¹, Alex K. Vaskov², Zachary T. Irwin¹, Phillip T. Henning³, Daniel R. Lueders³, Ann T. Laidlaw³, Alicia J. Davis⁴, Chrono S. Nu¹, Deanna H. Gates^{1,2,5}, R. Brent Gillespie^{2,6}, Stephen W. P. Kemp⁷, Theodore A. Kung⁷, Cynthia A. Chestek^{1,2,8,9,*†}, Paul S. Cederna^{1,7,*†}

Copyright © 2020
The Authors, some
rights reserved;
exclusive licensee
American Association
for the Advancement
of Science. No claim
to original U.S.
Government Works

Peripheral nerves provide a promising source of motor control signals for neuroprosthetic devices. Unfortunately, the clinical utility of current peripheral nerve interfaces is limited by signal amplitude and stability. Here, we showed that the regenerative peripheral nerve interface (RPNI) serves as a biologically stable bioamplifier of efferent motor action potentials with long-term stability in upper limb amputees. Ultrasound assessments of RPNI revealed prominent contractions during phantom finger flexion, confirming functional reinnervation of the RPNI in two patients. The RPNI in two additional patients produced electromyography signals with large signal-to-noise ratios. Using these RPNI signals, subjects successfully controlled a hand prosthesis in real-time up to 300 days without control algorithm recalibration. RPNI show potential in enhancing prosthesis control for people with upper limb loss.

INTRODUCTION

Upper limb loss can markedly alter an individual's lifestyle and impede his or her ability to perform activities of daily living. Building a direct interface to the peripheral nervous system could ultimately provide the best option for intuitive control of an upper limb prosthesis. However, current peripheral nerve interfaces have limitations, which minimize their clinical utility (1, 2). Electrodes placed within a peripheral nerve can record distinct efferent motor action potentials but over time are susceptible to decline in signal amplitude (3, 4). Instead, electrical stimulation has shown promise in providing tactile feedback through stimulation of afferent sensory axons (3, 5–7). Electrodes placed around a nerve have been successfully used in humans for improving sensory feedback for more than 2 years. These electrodes can be used to stimulate efferent motor axons to control distal innervated muscles and afferent sensory axons to provide patients with a sense of touch and pressure while using a prosthesis (8). However, recording specific efferent motor action potentials is challenging because of the small amplitude of the signals, limiting the number of independent control signals that can be recorded (9).

Targeted muscle reinnervation (TMR) can provide multiple control signals by transferring divided peripheral nerves in a residual limb to intact local or regional muscles. Surface electromyography (EMG) is then used to record the efferent motor control signals (10).

With TMR, a normally innervated muscle must be partially denervated to provide a new target for recording EMG signals from the implanted nerve. In addition, two or three nerves (median, radial, and ulnar) may be implanted into the same target muscle (for example, the pectoralis major muscle), making it difficult to record independent control signals from individual nerves or fascicles. Consequently, implanted amputees can control a limited number of independent movements (11).

To achieve both greater signal specificity and long-term signal stability, we have developed a regenerative peripheral nerve interface (RPNI). RPNI is composed of a transected peripheral nerve, or peripheral nerve fascicle, that is implanted into a free muscle graft (12, 13). The free muscle graft undergoes an approximately 3-month process of regeneration, revascularization, and reinnervation by the implanted peripheral nerve (12). This process creates a stable, peripheral nerve bioamplifier that produces high-amplitude EMG signals, which could be used to control a prosthetic device (14–17). In addition, RPNI have been shown to prevent and treat neuroma pain and phantom pain after amputation (18–20). To date, more than 200 patients have been implanted with RPNI for the prevention and/or treatment of neuroma pain and phantom pain. Here, we show that RPNI, implanted in participants with upper extremity limb loss, actively produced RPNI muscle contractions during volitional phantom finger movement. In addition, we successfully recorded independent efferent motor action potentials from RPNI, which provided real-time prosthetic finger control up to 300 days without recalibration of the control algorithm.

RESULTS

Clinical description and creation of the RPNI in upper limb amputees

Initially, seven participants with upper extremity amputations and symptomatic neuromas elected to undergo RPNI for the treatment of their neuroma pain and phantom pain and also elected to participate in a study involving the temporary placement of percutaneous

¹Department of Biomedical Engineering, University of Michigan, Ann Arbor, MI 48109, USA. ²Robotics Institute, University of Michigan, Ann Arbor, MI 48109, USA. ³Department of Physical Medicine and Rehabilitation, University of Michigan, Ann Arbor, MI 48109, USA. ⁴University of Michigan Hospital Orthotics and Prosthetics Center, Ann Arbor, MI 48109, USA. ⁵School of Kinesiology, University of Michigan, Ann Arbor, MI 48109, USA. ⁶Department of Mechanical Engineering, University of Michigan, Ann Arbor, MI 48109, USA. ⁷Section of Plastic Surgery, University of Michigan, Ann Arbor, MI 48109, USA. ⁸Department of Electrical Engineering and Computer Science, University of Michigan, Ann Arbor, MI 48109, USA. ⁹Neuroscience Graduate Program, University of Michigan, Ann Arbor, MI 48109, USA.

*Corresponding author. Email: cchestek@umich.edu (C.A.C.); cederna@med.umich.edu (P.S.C.)

†These authors contributed equally to this work.

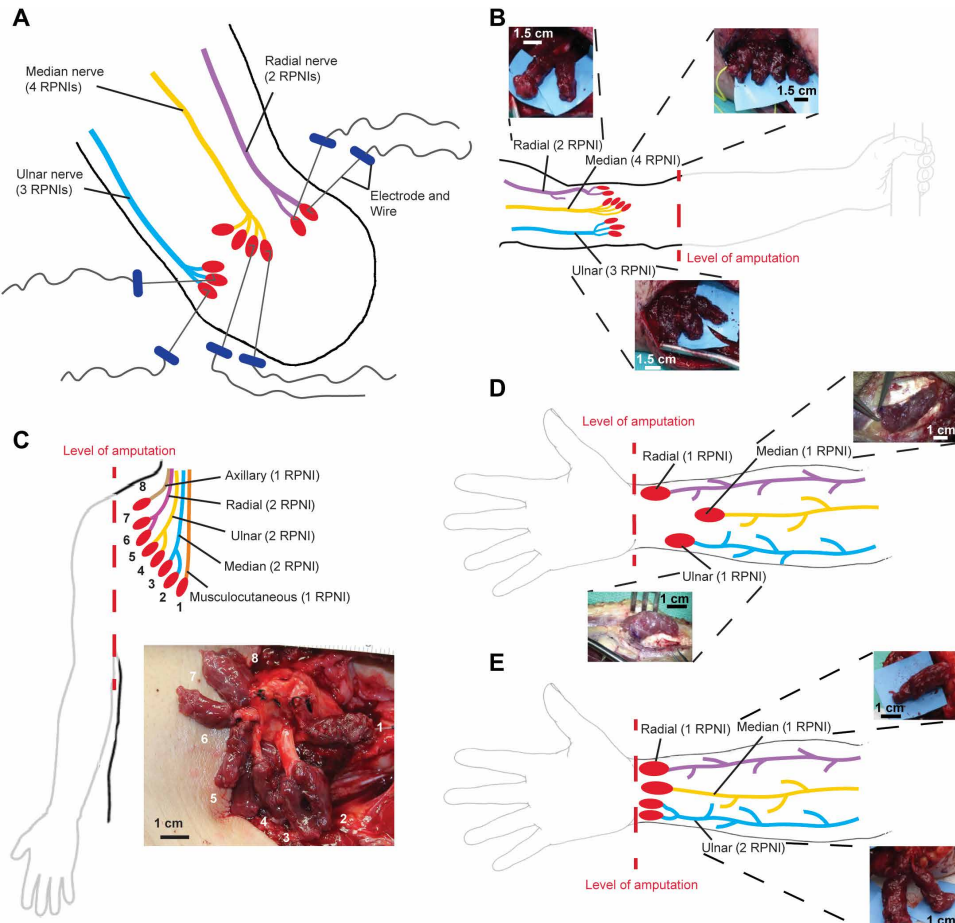


Fig. 1. Fine wire electrode insertion and anatomical illustrations of RPNI surgical creation. **(A)** Illustration of multiple RPNI s created for each available nerve. Percutaneous bipolar hook electrodes were embedded into the RPNI muscle belly of P1 during acute sessions. **(B)** P1 who had a proximal transradial amputation had nine RPNI s created: four for the median nerve, three for the ulnar nerve, and two for the radial nerve. **(C)** Illustration of the creation of P2's RPNI s at the glenohumeral amputation level. P2 had eight RPNI s created: two each for the median, ulnar, and radial nerves, and one each for the musculocutaneous and axillary nerves. **(D and E)** Both P3 and P4 had amputations at the distal transradial level. P3 had three RPNI s implanted, one on each of the median, ulnar, and radial nerves, whereas P4 had four RPNI s implanted, one on each of the median and radial nerve and two on the ulnar nerve.

fine wires into their RPNI s for prosthetic control (see Materials and Methods). After one to two sessions of fine wire implantation using needles, three participants opted to drop out of the study because of the pain caused by the needles. The remaining four participants are presented below. A $3 \times 1.5 \times 0.5$ -cm muscle graft was harvested from a healthy native donor muscle. For all participants mentioned below, free muscle grafts were harvested from their ipsilateral vastus lateralis. The distal end of a transected peripheral nerve in the residual limb was then sutured into the muscle graft. This created an enclosed biologic peripheral nerve interface. This procedure was then repeated to provide the desired number of RPNI s (Fig. 1A), which was different in each of the four participants because of unique aspects of their amputation.

Participant 1 (P1) is a 45-year-old male who sustained a left proximal transradial amputation. He was recruited 16 years postoperatively with severe, persistent neuroma pain that was inadequately treated using traditional techniques. In 2016, the patient underwent excision of his ulnar, median, and radial nerve neuromas at the level

of his antecubital fossa. An intraneuronal dissection of the median, ulnar, and radial nerves was performed to isolate individual nerve fascicles. We then implanted the end of each divided nerve fascicle into a separate muscle graft. Four RPNI s were created on the median nerve, three RPNI s on the ulnar nerve, and two RPNI s on the radial nerve (Fig. 1B). After RPNI surgery, P1 elected to undergo a temporary implantation of percutaneous fine wires to record efferent motor action potentials from the RPNI s (Fig. 1A).

P2 is a 72-year-old male who presented with a sarcoma on his right upper extremity. In 2018, he underwent a glenohumeral amputation, and RPNI s were created for neuroma prevention. An intraneuronal dissection of the median, ulnar, and radial nerves was performed to isolate individual nerve fascicles. Two RPNI s were created on each of the median, ulnar, and radial nerves, and one RPNI was created on the musculocutaneous nerve and one on the axillary nerve (Fig. 1C).

P3 is a 30-year-old male who sustained a traumatic amputation of the right hand, resulting in a right wrist disarticulation. He was recruited 2 years after his original injury with severe, persistent symptomatic neuromas of the median, ulnar, and dorsal radial sensory nerves. The pain limited his ability to wear his prosthesis. In 2015, P3 underwent resection of his median, ulnar, and dorsal radial sensory nerve neuromas in his distal forearm. One RPNI was created on each of these nerves (Fig. 1D). He elected to undergo implantation of indwelling bipolar electrodes in 2018, under a Food and Drug Administration investigational device exemption (fig. S1A).

P4 is a 53-year-old female who developed a urinary tract infection, leading to septic shock and acute renal failure. Her treatment was complicated by an intravenous extravasation of calcium into her right hand and forearm, leading to tissue necrosis and requiring a partial hand amputation. Her residual hand became progressively more contracted with limited active and passive range of motion of the interphalangeal (IP), metacarpal phalangeal, and wrist joints. In 2017, she underwent a voluntary distal transradial amputation. One RPNI was created on each of the median and radial nerves, and an intraneuronal dissection of the ulnar nerve was performed to create two RPNI s (Fig. 1E). One year after the RPNI surgery, P4 elected to undergo implantation of indwelling bipolar electrodes (fig. S1B).

Observed muscle contractions of the RPNI

Two participants (P1 and P2) with RPNI s created above the elbow (that is, no long flexors or extensors of the fingers or wrist remain) were evaluated with ultrasound, and their RPNI s were observed to

contract during phantom finger movements. Participants were asked at the beginning of each behavioral task whether they could move the fingers of their phantom limb. In this situation, the RPNIIs were observed contracting during movement of the phantom fingers. Figure 2 shows sonograms with RPNI contractions highlighted according to the anatomical movement that was observed under ultrasound.

Specifically, P1's median nerve RPNIIs are located near the short head of the biceps brachii, proximal to the elbow with no finger-related musculature remaining. These median nerve RPNIIs, identified by ultrasound, demonstrated independent contractions during attempted

thumb IP and index finger proximal IP (PIP)/distal IP (DIP) joint flexion of the phantom limb (movie S1). Specifically, median RPNI 1 contracted for thumb flexion, whereas median RPNI 2 to RPNI 4 and a subsection of RPNI 1 contracted for index finger flexion (Fig. 2A). These contractions were associated with minimal movement of the surrounding tissue. At this level of amputation, these were anatomically anticipated movements associated with the median nerve (table S1).

P1's ulnar RPNIIs were located near the long and medial heads of the triceps brachii. The bulk of RPNI 1 and RPNI 2 contracted

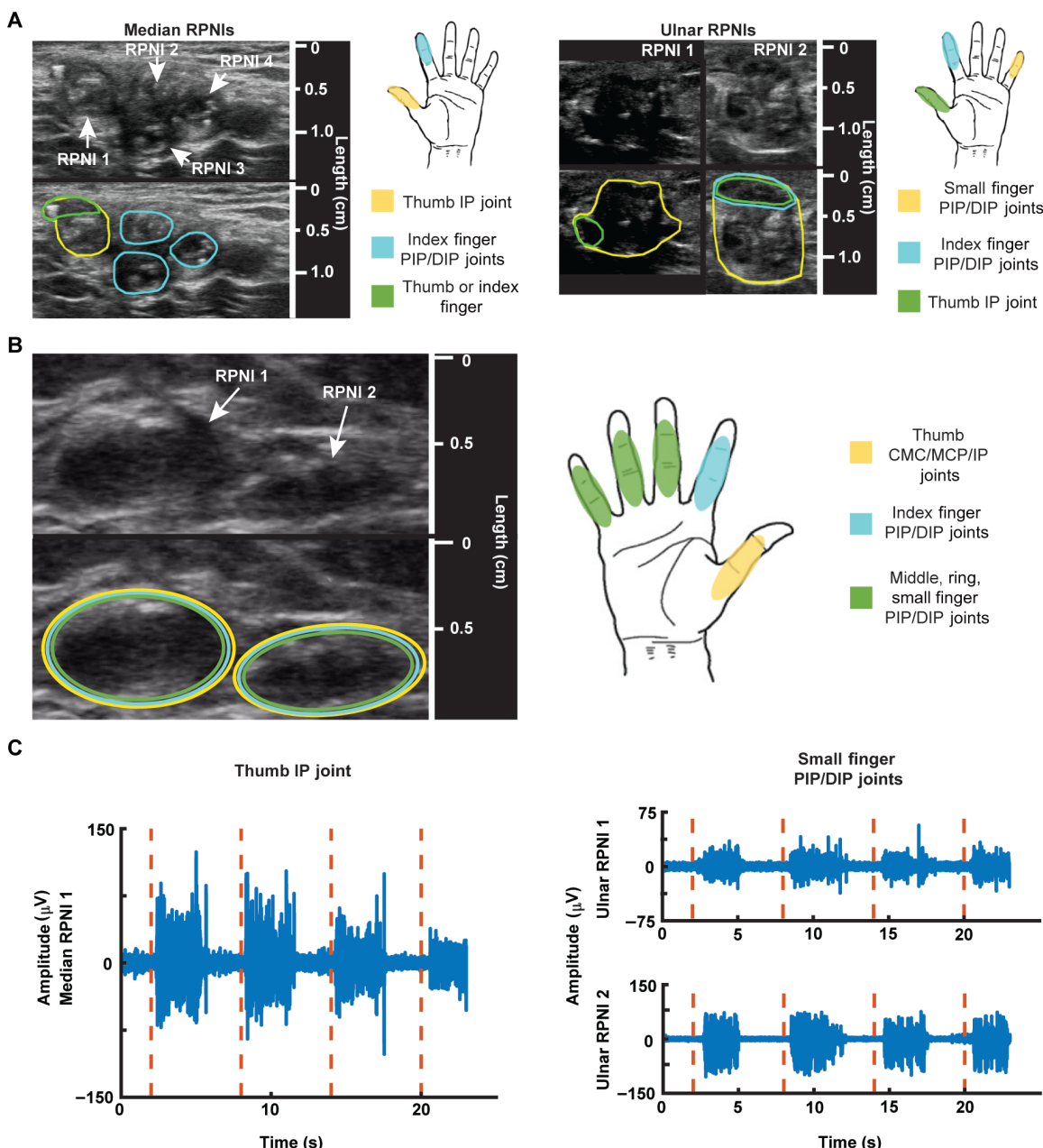


Fig. 2. RPNI sonograms, motor map, and electrophysiology. (A) P1's median and ulnar RPNI sonograms captured 19 months after RPNI surgery. Encircled areas on the sonogram show which region of the median or ulnar RPNIIs contracted during cued finger movements. (B) P2's sonogram of two RPNIIs captured 8 months after RPNI surgery and motor map of active areas. (C) P1's EMG signals (blue) recorded from median RPNI 1 after cued thumb IP joint movement (red dashed line), and EMG signals (blue) recorded from ulnar RPNI 1 and RPNI 2 after cued small finger PIP/DIP movement (red dashed line).

during volitional small finger PIP/DIP joint flexion of the phantom hand, whereas a subsection of both RPNIIs contracted for thumb movement (Fig. 2A and movie S2). These movements were also anatomically expected as the ulnar nerve innervates muscles controlling small finger and thumb movements. A small subsection of the ulnar RPNI did appear to undergo small but visible contractions during volitional index finger movement. This was anatomically unexpected but may be due to P1's 16-year period without a hand, making certain volitional movements difficult to generate independently.

Unlike P1, P2 underwent an amputation at the shoulder level where the functionalities and segregation of the hand's median, ulnar, and radial nerves are mixed and undefined. Nonetheless, RPNI contractions were still observed during finger-related movements. In particular, two RPNIIs were unambiguously identified because of their sutures near the lateral side of the right pectoralis major. With some variation in amplitude, they contracted during thumb carpometacarpal (CMC)/metacarpophalangeal (MCP)/IP joint flexion, index PIP/DIP joint flexion, and middle, ring, small finger PIP/DIP joint flexion (Fig. 2B and movie S3). These RPNI contractions, seen in two participants missing finger-related musculature, suggest that nerves carrying efferent motor action potentials controlling finger functionality successfully reinnervated the RPNIIs, allowing P1 and P2 to have volitional control over their phantom hand.

To perform a statistical comparison of the RPNIIs to the surrounding tissue, we evaluated mean pixel intensity within the RPNIIs versus the surrounding tissue (Wilcoxon rank sum test). Overall, P1's median RPNI 1 and ulnar RPNI 1 and RPNI 2 had a significant change in mean pixel intensity than the surrounding tissue during thumb and small finger flexion, respectively ($P < 0.001$ for both comparisons). For index finger flexion, median RPNI 1 contracted more than the surrounding tissue ($P < 0.001$), whereas observation of median RPNI 2 to RPNI 4 demonstrated smaller contractions and had mixed pixel changes (table S2).

To verify that these contractions had associated EMG, we recorded from these RPNIIs using percutaneous fine wires. P1, but not P2, elected to have these wires inserted. The bipolar wire electrodes have a 1-mm distance between contacts to record from a localized area of the RPNI. Here, we observed clear EMG spikes associated with thumb movements in median RPNI 1, with a signal-to-noise ratio (SNR) of 4.62, and for small finger movements in ulnar RPNI 1 and RPNI 2 (mean SNR = 3.80) (Fig. 2C). This suggests that these RPNI grafts amplify efferent motor nerve action potentials, actively contract, and generate EMG signals similar to residual muscle.

In P3 and P4, who had RPNIIs in their distal forearm, ultrasound was used to easily locate the RPNIIs (fig. S2). However, because of the motion of the surrounding innervated residual muscles, dedicated RPNI movement was difficult to isolate because of the contractions and conformational changes of the adjacent innervated residual muscle.

Surgically implanted indwelling bipolar electrodes

P3 and P4 elected to undergo implantation of indwelling bipolar EMG electrodes. In these patients, we evaluated the ability of the RPNIIs to amplify efferent motor action potentials and to provide these motor control signals long term. In both participants, large amplitude, anatomically appropriate motor control signals were recorded from the indwelling RPNI electrodes ($n = 2,3$).

P3 had one median RPNI and one ulnar RPNI, whereas P4 had a single median RPNI and two ulnar RPNIIs. EMG envelopes for six

different phantom limb movements are shown in (Fig. 3). The averaged peak-to-peak amplitude for the most preferred movement on the RPNIIs was 2.77 ± 0.660 mV with an SNR of 102 and 501 ± 145 μ V with an SNR of 36.1 on P3's median and ulnar RPNIIs, respectively (fig. S2, A and B). Likewise, P4's median nerve RPNI had an average peak-to-peak amplitude of 579 ± 209 μ V (SNR = 19.1), ulnar nerve RPNI 1 had an amplitude of 334 ± 80.9 μ V (SNR = 15.6), and ulnar nerve RPNI 2 had an amplitude of 501 ± 164 μ V (SNR = 28.3) (fig. S2, C and D). These electrodes had a larger spacing between the bipolar contacts (10 mm) than the percutaneous fine wire electrodes (1 mm). The more accurate surgical targeting of the bipolar indwelling electrode into the RPNI may account for the larger amplitude efferent motor action potential signals compared with P1.

RPNI signal recording specifically identified physiologically correct motions from each of the peripheral nerves in both participants. As expected, there was minimal median nerve RPNI signal detection during small finger flexion (Fig. 3, A and B). For the ulnar nerve RPNIIs, RPNI activation appropriately occurred during flexion of the phantom thumb, whereas minimal activation occurred during index finger flexion. In addition, the ulnar nerve RPNIIs activated for finger abduction/adduction; anatomically, these finger motions are exclusively controlled by the ulnar innervated intrinsic muscles of the hand (Fig. 3, A and B). The split ulnar grafts in P4 had different activation patterns. Ulnar RPNI 2 was more strongly activated during finger abduction/adduction and thumb CMC/MCP joint motion than ulnar RPNI 1 (Fig. 3B). These findings suggest that efferent motor action potentials can be recorded using RPNIIs from individual nerve fascicles, each of which may have distinct and unique motor control signals.

Real-time myoelectric prosthetic control

The observed high-amplitude RPNI signals and unique activation patterns suggested that these signals would be useful for prosthetic hand control. We first evaluated this possibility using a pattern recognition approach (see Materials and Methods), testing whether RPNI-generated signals could discretely predict hand postures. Using a simple naïve Bayes classifier trained with only RPNI signals, we were able to decode five different finger postures in each subject, both offline and in real time (Fig. 4). When the classifier was trained with both RPNI signals and residual muscle signals (see Materials and Methods), we were able to decode four different grasping postures (fig. S3). During real-time control, P3 was able to control the virtual thumb opposition and flexion, as well as small finger flexion, finger adduction, and resting hand postures with 100% accuracy (Fig. 4A and movie S4). P4 was able to control the ring finger, thumb flexion, small finger, finger abduction, and resting hand postures with 94.3% accuracy (Fig. 4B and movie S5). In addition, each subject was able to control fist, pinch, point, and extend fingers with 100% accuracy (fig. S3, A and B, and movie S6). Offline decoding alluded to these high-accuracy, real-time predictions in both participants (Fig. 4, C and D, and fig. S3, C and D). The majority of movements were selected quickly, with the fastest motion selection times, or the times between EMG onset and the classifier's prediction, less than 0.3 s (Fig. 4, A and B). P3 and P4's averaged motion selection time across all movements were 0.172 ± 0.105 and 0.234 ± 0.0894 s, respectively (means \pm SD; table S3).

We next tested whether P3 and P4 could voluntarily modulate the RPNI signals to continuously control the finger position of the virtual hand's thumb. Using a regression approach (see Materials and Methods), we asked each participant to hit 2-cm spherical targets

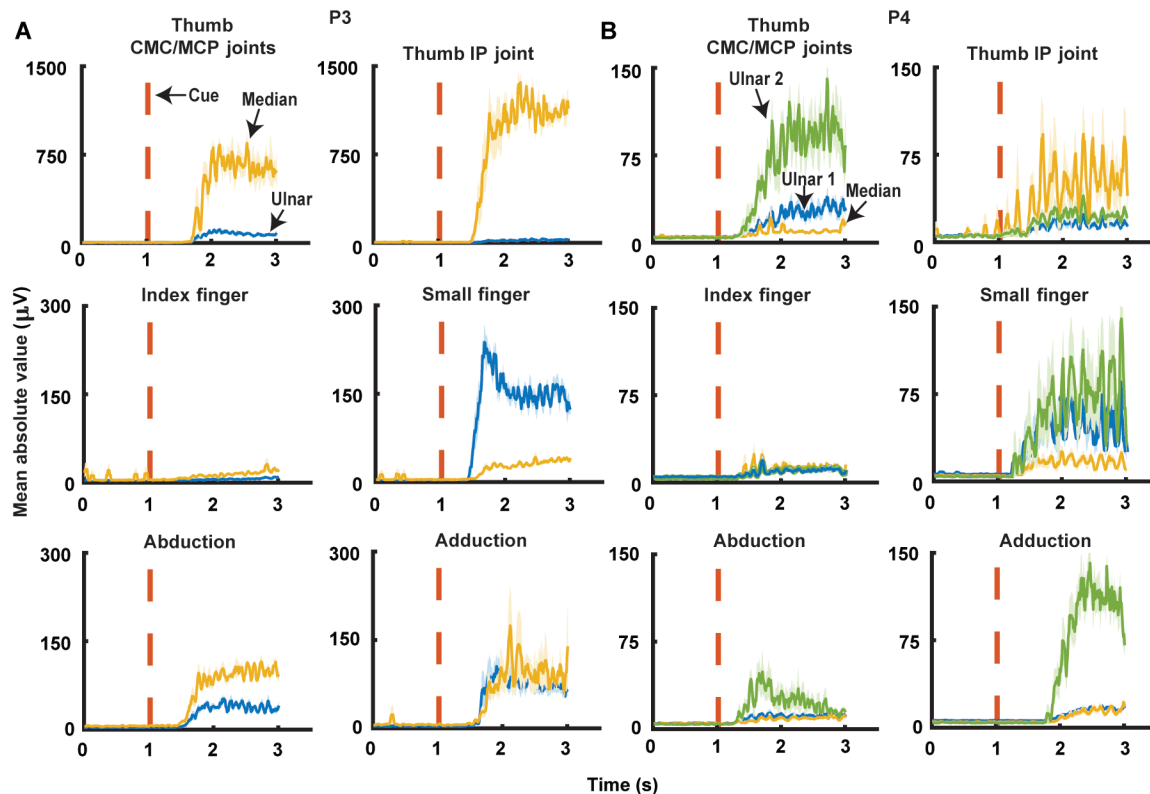


Fig. 3. RPNI mean absolute value signals during six different finger movements. (A) P3's median and ulnar RPNI MAV signals during thumb carpometacarpal (CMC)/metacarpophalangeal (MCP) joint flexions, thumb interphalangeal (IP) joint flexion, index finger MCP/proximal interphalangeal (PIP), small finger MCP/PIP joint flexions, hand abduction, and hand adduction movements. (B) P4's median RPNI, ulnar RPNI 1, and ulnar RPNI 2 MAV signals during thumb CMC/MCP joint flexions, thumb IP joint flexion, index finger MCP/PIP joint flexions, small finger MCP/PIP joint flexions, finger abduction, and finger adduction movements.

placed along the virtual hand's range of motion. P3 and P4 acquired targets with 100 and 96.3% accuracy on day 0, respectively. To test P3 and P4's performance across time, the algorithm's parameters trained on day 0 were reused across multiple days, up to 300 days for P3 and 97 days for P4. On the last day, P3 and P4 were still able to acquire targets with high accuracy, 100 and 96.4%, respectively (Fig. 5, A and B, and movies S7 and S8). In addition, extraction of single motor units from P3 and P4's median RPNI showed signal amplitude variability from day to day, ± 17.2 and $\pm 6.63\%$, respectively, but no observable decreasing trend in amplitude (Fig. 5, C and D). Previously, we found similar signal variability, which affected RPNI motor performance in nonhuman primates (14). In this study, however, we did not observe a change in motor performance in either subject.

To further increase the degree of functionality, we simultaneously controlled the thumb IP joint and thumb CMC/MCP joints as a two degree of freedom (DOF) thumb. P3 and P4 performed the same target hitting task in these two axes, hitting eight targets with 100 and 97.2% accuracy with an average time to success of 0.987 ± 0.16 and 2.83 ± 0.43 s, respectively (Fig. 5, E and F, and movie S9). As a direct comparison, P4 performed the same task using surface EMG (see Materials and Methods), hitting targets with 78.4% accuracy with an average time to success of 4.40 ± 0.50 s (movie S10). Surface EMG amplitude was lower than intramuscular EMG, which may have contributed to the decrease in performance. In addition to the virtual target task, P3 was asked to use the physical prosthesis (LUKE arm, Deka) to touch the tip of a wand, placed at different

locations, with the tip of the prosthetic thumb (Fig. 5G). The high accuracy of the thumb control seen during the virtual task translated well to the physical prosthesis (movie S11).

To test functional control, P3 and P4 were both fitted with a custom socket to perform functional tasks. A one DOF index finger using signals from his flexor digitorum profundus to the index finger (FDPI) was added to P3's simultaneous two DOF thumb control. The participant used this three DOF control to complete a self-paced box and blocks task (movie S12). P3 reported intuitive control while navigating the thumb and index finger to precise positions. Because of the weight, P4 was unable to lift the LUKE hand to complete the functional tasks. Consequently, we used an extra small i-limb Quantum. P4 used a two DOF control strategy built to predict thumb and small finger flexion, which were then mapped to proportionally control key pinch and power grip. The subject successfully and sequentially completed a trio of Southampton Hand Assessment Procedure (SHAP) abstract tasks (movie S12). For both subjects, we quantitatively compared the predicted finger positions during the functional tasks to offline simulated predicted positions using only recorded EMG from implanted residual muscles. The normalized average Euclidean distance between P3's real-time predicted two-dimensional thumb trajectory and simulated two-dimensional thumb position trajectory was 25.5% of the maximum range of motion during active thumb periods (fig. S4A). P4's real-time and simulated thumb position differed by 53.8% during active thumb periods (fig. S4B). There was a significant difference between the original and

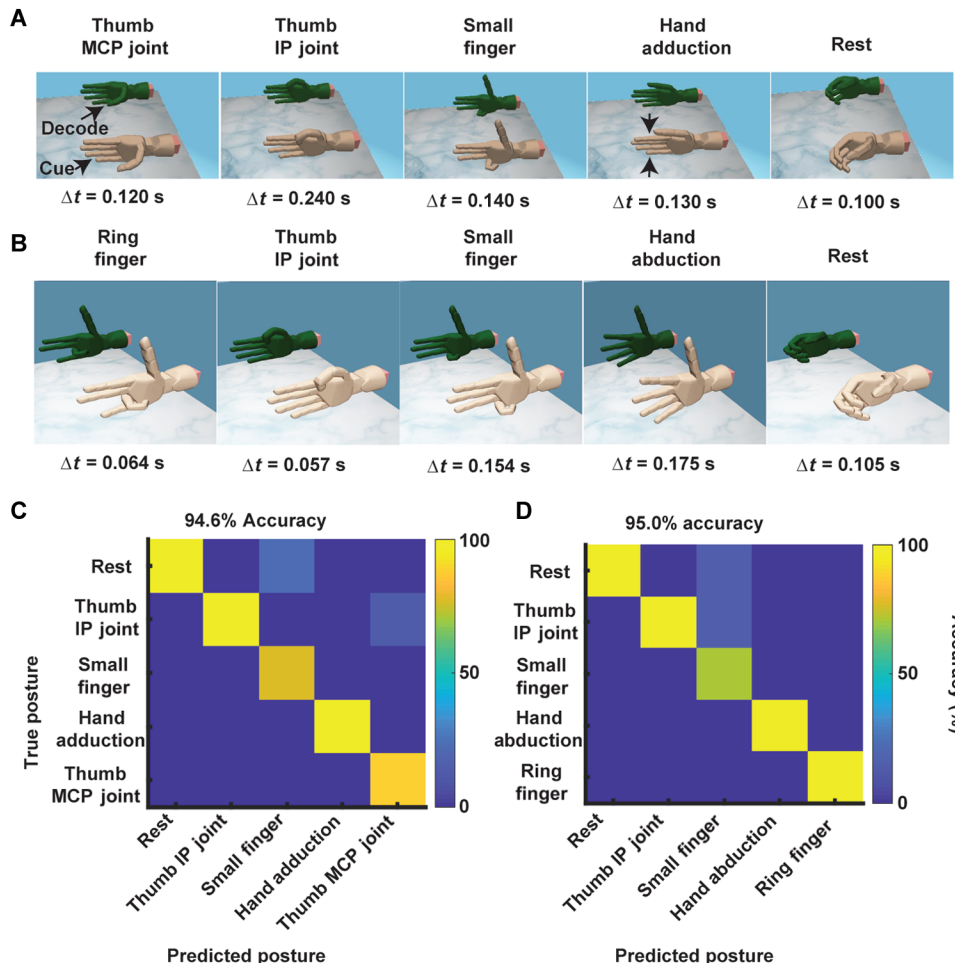


Fig. 4. Real-time classification of finger movements. (A and B) P3 and P4's discrete control of thumb MCP joint (opposition), thumb IP joint (flexion), small finger, adduction, and rest for P3, and ring finger, thumb IP joint, small finger, abduction, and rest for P4. The fastest motion selection times are shown for each posture. (C and D) Offline confusion matrix of the postures used in (A) and (B), respectively. The y axis represents the true posture, whereas the x axis represents the predicted posture. The color map indicates the accuracy (%) of the classifier's prediction.

simulated trajectories ($P < 0.001$), which suggests that the RPNI signals played an important role in contributing to the subject's intentional thumb movement.

DISCUSSION

We have shown in four upper limb amputees that RPNI might be an effective peripheral nerve interface to provide efferent motor signals for control of prosthetic devices. The RPNI amplifies efferent nerve signals to provide favorable SNRs for high-fidelity control of both extrinsic and intrinsic hand functions. The SNR of the recorded EMG had a mean of 4.21 in P1, 68.9 in P3, and 21.0 in P4. The wide SNR gap between P1, P3, and P4 is likely due to the smaller bipolar electrode spacing in acute fine wires (1 mm) versus indwelling EMG electrodes (10 mm), whereas the difference between P3 and P4's measured SNR may be due to the period of reinnervation. P3's nerves had an additional 2 years to reinnervate his muscle grafts before electrode implantation. Nonetheless, P3 and P4's SNRs were substantially larger for RPNI with implanted bipolar electrodes than measured SNR in nerve cuff electrodes or intraneuronal probes, whose

SNR ranges from 4 to 15 (3, 9, 21, 22). In addition, intraneuronal probes, such as the Utah slanted electrode array, can provide large signals but currently run into issues of signal stability over time (4). In comparison, RPNI have remained a stable peripheral nerve interface for 2 years in P1, 8 months in P2, 3 years in P3, and 1 year in P4. The chronic bipolar electrodes used in this study are similar to those that have been previously observed to record stable EMG for up to 7.5 years (23). As P3 and P4 remain implanted, we hypothesize that RPNI signals will continue to demonstrate stability over the course of their implantation. Although surface electrodes recorded smaller amplitude EMG signals than intramuscular electrodes, this does not entirely eliminate the possibility of using surface electrodes to record RPNI signals. A modified surgery could be performed in which the RPNI are placed closer to the skin, allowing a greater chance of recording higher-amplitude surface EMG signals.

With ultrasound guidance, we demonstrated that different subregions of each RPNI contracted for different volitional movements. This is in line with the idea that the reinnervated muscle of the RPNI will have different single motor units reinnervating distinct portions of the free muscle graft. With surgically implanted indwelling electrodes at the distal transradial level, we have shown that RPNI EMG activation occurred during specific intrinsic hand movements. Together, this suggests that RPNI are functionally

selective. To gain even greater selectivity for prosthetic control, electrodes with more recording sites within RPNI can theoretically provide enhanced signaling. In contrast to intraneuronal electrodes, which require numerous recording sites a few hundred micrometers apart, electrodes in RPNI could have recording sites millimeters apart to record different efferent motor control signals.

In previous studies, investigators have provided prosthetic control signals by interfacing with intact muscles in the residual limb. This strategy has provided reasonable signal amplitude and some control of a prosthetic limb in patients undergoing transradial amputations (24–28). However, when intrinsic hand muscles and extrinsic flexors and extensors of the fingers are absent, there is no effective way to obtain these control signals without directly interfacing with the peripheral nerves. RPNI have provided an alternative where directly extracting efferent motor action potentials from the peripheral nerve is possible. Furthermore, we did not need to transect any nerve branches to any of the residual muscles of the upper arm and, thus, did not denervate existing muscle, as is necessary in TMR (29).

The most promising finding of intrinsic hand functionality was the ability for P3 and P4 to control the intrinsic muscles of their thumb

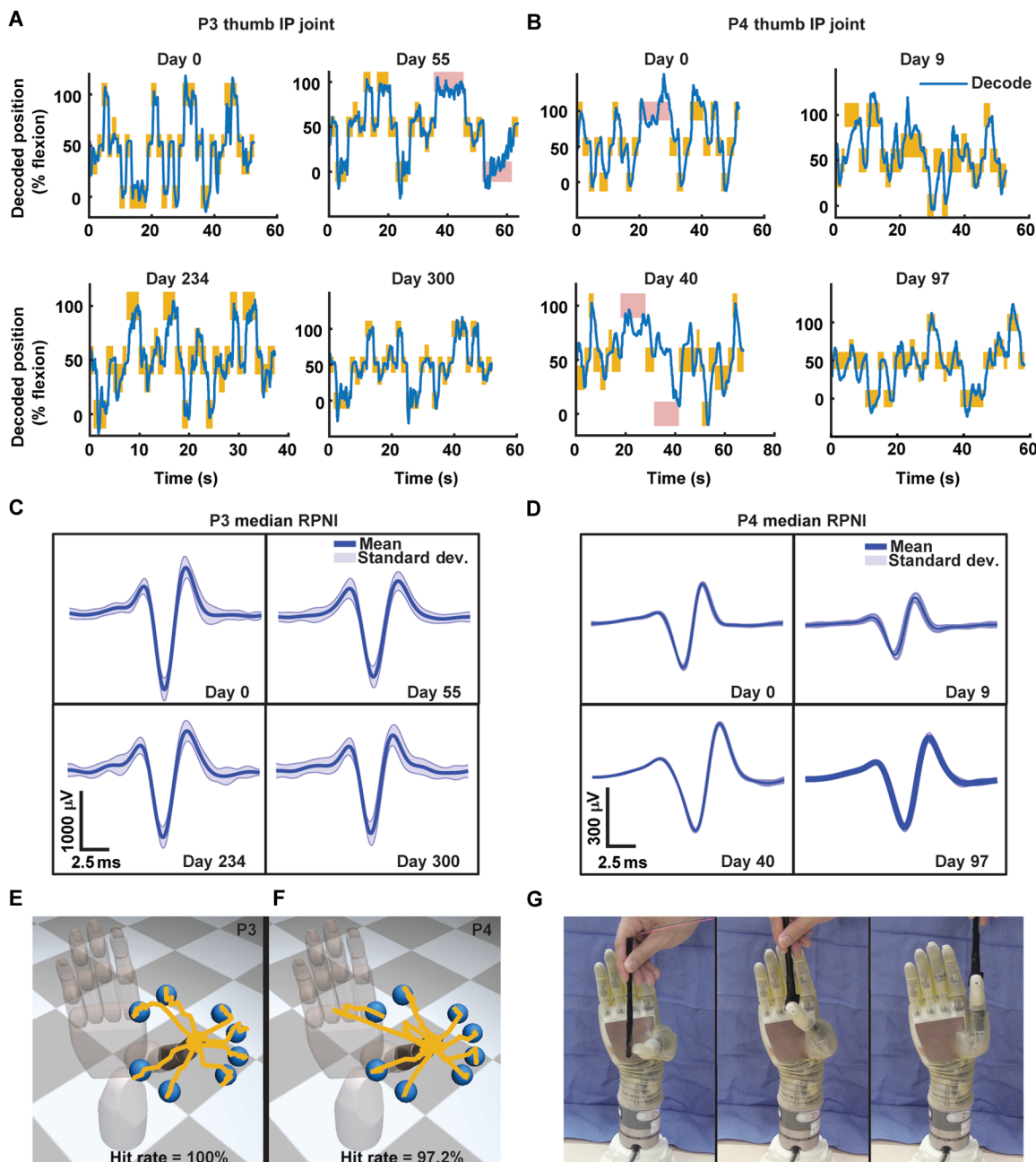


Fig. 5. Real-time continuous control of the virtual and physical prosthesis. (A and B) Examples of P3 and P4's real-time predicted trajectories (blue) for one DOF thumb IP joint movement across multiple days using a one-time calibrated decoding algorithm. The y axis represents the percentage of flexion, 0% equals finger fully extended, 50% equals finger at rest, and 100% equals finger fully flexed. Each maize rectangle indicates the target was successfully acquired, whereas red rectangles indicate unsuccessful trials. The width of the rectangle represents how long the virtual target was displayed, whereas the height represents the size of the virtual target. (C and D) Single motor units extracted across days from the median RPNIs of P3 and P4. Blue and shaded trace represents mean and SD of extracted units. (E and F) Example of predicted trajectories during real-time two DOF continuous decoding of thumb CMC/MCP/IP joint movements in virtual space. (G) An equivalent target hitting task in physical space using the LUKE arm (Deka).

using both their ulnar and median RPNIs. This is anatomically appropriate since both the median and ulnar nerves innervate several intrinsic muscles, which assist in flexing the thumb CMC/MCP joints. Previous studies of simultaneous control of multiple DOFs have focused on controlling the wrist and hand open/closed (26, 28, 30). In this study, RPNIs enabled P3 and P4 to have intuitive two-axis thumb

control including thumb flexion/extension and thumb opposition/reposition. These additional control signals combined with existing residual muscle may help gain more dexterous control of the prosthetic hand, as many studies are limited to capturing motor signals from residual musculature (28, 31–35). As demonstrated during functional tasks, continuous control of three DOFs was achieved by

adding residual EMG from the FDPI muscle. However, further testing is warranted to directly compare continuous and pattern recognition controllers for real-world tasks. To date, pattern recognition controllers have outperformed conventional controllers during standardized functional trials (36). This suggests that pattern recognition controllers will still be needed until a more robust continuous controller is developed. For future work, we plan to further explore the capabilities of combining RPNIIs with residual innervated muscles to extend control to greater DOFs. EMG-driven musculoskeletal models have been developed for real-time, physiologically accurate prosthesis control during functional tasks (30) but have only shown control of two to three DOFs. We postulate that the number of residual muscle signal sources is a limiting factor in these models and that additional signal sources from the RPNIIs could potentially increase prosthesis controllability and functionality.

In addition to prosthesis control, RPNIIs have shown to be an effective technique to reduce symptomatic neuroma pain and also prevent neuroma formation (18–20). Similar results have been demonstrated with TMR (37), with a more recent study providing evidence that TMR decreases phantom limb pain (38). Additional studies should compare the relative efficacy of each technique in reducing both neuroma and phantom limb pain. Furthermore, RPNIIs may provide a potential sensory component that could bring tactile and proprioceptive feedback to prosthetic users. Adding a sensory component would build a robust bidirectional closed-loop prosthetic paradigm, theoretically improving motor functionality and giving individuals a sense of embodiment (3, 8).

This pilot study has demonstrated that the RPNI technique can be a viable clinical option to improve prosthesis control for upper extremity amputations, although limitations of the study should be noted. Our study design did not include a direct comparison to other surgical approaches (for example, TMR). A future study is warranted to determine whether one approach has more clinical benefits than the other. In addition, we were limited in the number of intramuscular electrodes that we could implant for safety reasons. This led to a careful decision on which residual muscles to implant to provide the best prosthesis control for the subjects. To further explore the contributions of RPNI signals at the transradial level, future study designs should consider implanting into all relevant residual muscles to compare prosthetic performance with and without RPNI signals.

We have demonstrated that RPNIIs can be used to record efferent motor nerve action potentials at both the intrinsic and extrinsic stages. RPNIIs have shown proficiency in amplifying motor nerve signals, enabling motor selectivity, allowing smooth continuous control of one and two DOF thumb movements, and remaining a stable peripheral nerve interface over time. Thus, the RPNI technique combined with a wireless recording/stimulation device may revolutionize future clinical prosthetic technology and greatly improve the quality of life for patients with limb loss.

MATERIALS AND METHODS

Study design

This study investigated whether the RPNI procedure can amplify efferent nerve action potentials to provide unique stable signals for control of one and two DOF finger prosthesis. The experiments presented were designed to demonstrate the RPNI's viability in human subjects, determine the long-term stability of one DOF motor performance, and improve volitional control of a virtual and physical

hand prosthesis for functional tasks. Ultrasound imaging and electrophysiological recordings were used to measure RPNI viability, and virtual and physical prosthetic hand control tasks were performed to measure motor performance. This was a first-in-human, nonblinded, nonrandomized pilot study. No power analysis was calculated before the study. Participants were selected for the treatment of neuroma pain or prevention of neuroma growth. Ultrasound imaging was replicated across all four subjects, electrophysiological recordings across three subjects, and prosthesis control tasks across two subjects. The Institutional Review Board at the University of Michigan approved this study, and each participant provided written and informed consent.

Electrophysiology

P1, P2, P3, and P4 participated in experimental sessions beginning 4, 8, 6, and 11 months after RPNI surgery, respectively. Initiation of experimentation was based on patient availability and results from previous animal work, which demonstrated that it took approximately 3 months for RPNIIs to mature and stabilize (12, 15–17). During each experiment, ultrasound imaging was performed to identify and measure the RPNIIs with the option for participants to have guided percutaneous fine wire electrodes placed into the RPNIIs (Natus Medical P/N 019-475400). In addition, fine wire electrodes were also placed percutaneously into available innervated muscles in the residual limb. The electrodes were removed at the completion of each session.

After completing the fine wire sessions, P3 and P4 elected to undergo surgical implantation of eight indwelling intramuscular bipolar electrodes (30.5 × 0.025 cm, Synapse Biomedical). The electrodes consist of two stainless steel leads coiled in a double helix formation and insulated with perfluoroalkoxy material. For P3, electrode implantation was performed 3 years after the original RPNI surgery and 5 years after the original amputation. One electrode was implanted in each of the median and ulnar nerve RPNIIs (fig. S1A). For P4, electrode implantation was performed 12 months after the original RPNI and amputation surgery. Like P3, P4 had one electrode implanted in each RPNI (fig. S1B and table S4). No electrode was implanted into the dorsal radial sensory RPNI for either participant, since it is a purely sensory nerve and transduces no efferent motor action potentials. A neural signal processor (NeuroPort, Blackrock Microsystems) filtered EMG signals from RPNIIs between 3 and 7000 Hz (unity gain) and recorded the signals for offline analysis. For all three participants, EMG SNR was calculated offline. Specifically, the root mean square (RMS) of the EMG was divided by the RMS of the electrode's noise floor seen during rest. Peak-to-peak amplitude was calculated by taking the difference between the maximum and minimum EMG values. The SNR and peak-to-peak amplitude are calculated from 2 recording sessions with fine wire electrodes in P1, 13 sessions with indwelling electrodes in P3, and 9 sessions in P4.

Ultrasound imaging and recording

During ultrasound experiments, a 15–6 MHz linear array ultrasound transducer (SonoSite X-Porte) was positioned along the transverse plane of the arm to locate and measure the size of the RPNIIs in each participant. In addition, the subjects were asked to perform finger movements with their phantom hand, and the changes in the size and shape of the associated RPNIIs were evaluated and visualized. P1 volitionally flexed and extended his phantom thumb at a self-paced frequency of 1.5 Hz for a duration of about 13 s. Subsequently, he was asked to move his phantom index and then his phantom small

finger in a similar manner. P2, who had a glenohumeral amputation, was asked to volitionally flex and extend his phantom thumb, index, middle, ring, and small finger for approximately 30 s while following cued instructions from a researcher. Each ultrasound video clip was evaluated qualitatively and quantitatively.

To quantify the contraction of the RPNI, frames at rest and at maximum volitional contraction (MVC) of each video were analyzed, and the percentage difference of pixel mean intensity (MI) and SD between frames was calculated. Using MATLAB (MathWorks), the selected frames were segregated and labeled as rest or MVC. Subsequently, the manually traced RPNI region was extracted from each frame, and the remaining area was identified as the “surrounding tissue.” Similar calculations of the pixel MI and SD were taken as well as the percent differences between frames. This metric is an indicator of how much the selected region moved between rest and MVC. Ultrasound data were collected in two sessions in P1 and one session in P2.

Online prosthesis control

A continuous task and discrete task were conducted to measure motor performance. Each task was split between two phases: a training phase and a decoding phase. Only P3 and P4 performed both tasks using signals from the intramuscular bipolar electrodes.

For the continuous task training phase, participants performed a bilateral mirrored behavioral task in which finger position from their intact hand and EMG data from their amputated limb were recorded (34). Participants donned a glove embedded with five flex sensors (Spectra Symbol) on their intact hand to measure finger position. Using the glove, they controlled a virtual prosthetic hand generated by MuJoCo software and followed a visual target during a center-out target task (39). Participants followed the visual target for 2 to 5 min (~50 to 200 trials) and held the fingers of their intact hand and phantom hand within the target for 1 s. The target color would turn green if the participant successfully placed the virtual finger within the target radius. In addition, each trial was labeled success if the participant held the finger within the target for 1 s. To quantify the performance, we measured the accuracy and time to successfully acquire targets.

During this training phase, a neural signal processor (NeuroPort, Blackrock Microsystems, Salt Lake City, UT, USA) filtered EMG signals from residual muscles and RPNI between 3 and 7000 Hz (unity gain) and recorded the signals for offline analysis. The signals were then sent to xPC target where they were further filtered from 100 to 500 Hz. The real-time computer calculated the mean absolute value (MAV) from the EMG waveform (10, 35). In addition, the real-time computer received and smoothed the finger position data from the glove. Both the temporal features and the finger position data were stored in MATLAB to train a position/velocity Kalman filter, a machine learning algorithm previously shown to effectively interpret RPNI signals for continuous prosthetic control (14). A separate computer smoothed the stored MAV feature and finger position in successive 50-ms bins for P3 and 100-ms bins for P4 and calculated Kalman filter matrix coefficients. Offline Kalman filter analysis showed that the 100-ms bins gave P4 the best decoding performance. The coefficients were then uploaded to the real-time computer for use during the decoding phase.

To train one DOF thumb control, P3 and P4 were asked to volitionally flex and extend their phantom thumb IP joint. P3 and P4’s decoding EMG features were extracted from the median RPNI, and

a thumb-related intact extensor muscle (extensor pollicis longus) also implanted with an intramuscular bipolar electrode. To train two DOF thumb control, we asked P3 and P4 to first independently move their thumb IP joint and then independently move their thumb CMC/MCP joints (opposition/reposition). We then asked them to do movements that required all three joints: thumb CMC, MCP, and IP joints. The decoding EMG features used included all RPNI signals and intact extensor muscles (extensor pollicis longus and extensor digitorum communis). Training the Kalman filter followed a similar procedure found in Vu *et al.* (14). Briefly, the Kalman filter is a recursive linear filter that tracks the state of a dynamical system over time, relying on a trajectory model and an observation model. In the case of two DOF thumb control, the Kalman filter’s trajectory model represents the transition of the kinematic state of the thumb at time t to time $t + 1$. We assume that the thumb state vector \mathbf{x}_t represents the position and velocity of the thumb flexion/extension and thumb opposition/reposition.

$$\mathbf{x}_t = [pos_{thumbFlex}, pos_{thumbOpp}, vel_{thumbFlex}, vel_{thumbOpp}, I]^T \quad (1)$$

The observation model represents the transformation of the current thumb state to recorded EMG activity from the RPNI and residual extensor muscles. Here, MAV represented the temporal characteristics of the EMG waveform. If we let $\vec{\mathbf{y}}_t = [y_1, \dots, y_k]^T$, where y_k is the temporal feature of the k th electrode, then the linear relationship between the finger state and neural measurements is

$$\vec{\mathbf{x}}_t = \mathbf{A} \vec{\mathbf{x}}_{t-1} + \vec{\mathbf{w}}_t \quad (2)$$

$$\vec{\mathbf{y}}_t = \mathbf{C} \vec{\mathbf{x}}_t + \vec{\mathbf{q}}_t \quad (3)$$

where $\mathbf{A} \in R^{5 \times 5}$ and $\mathbf{C} \in R^{k \times 5}$ represent the trajectory and observation models. \mathbf{A} is the linear transformation from the previous finger state to the current finger state (the trajectory model), whereas \mathbf{C} is a mapping of the current finger state to the EMG temporal features (the observation model). The predicted thumb flex and thumb opposition position from \mathbf{x}_t controlled the LUKE arm’s thumb flex and thumb opposition, respectively. Because the glove did not measure thumb opposition/reposition, a real-time computer (MATLAB xPC target) controlled the movements of the virtual thumb, and P3 and P4 were instructed to follow along. P3 followed this protocol for the two DOF thumb training phase, whereas P4 followed this training protocol for all her one and two DOF training phases.

During the decoding phase, the Kalman filter allowed participants to volitionally control the virtual prosthetic finger in real time during the center-out target task. The participants performed the same task but without the data glove. The neural signal processor sent the filtered EMG signals from the RPNI and the extensor muscles to the xPC target where the MAV features were calculated, smoothed, and used to decode (predict) the participant’s volitional movement in real time. Participants used this decoder to control the virtual prosthetic finger between 20 and 100 trials. For one DOF movements, participants were required to hold the thumb within 2-cm targets for 1 s. During the two DOF control, participants were required to hold within 3-cm targets for 500 ms. The physical LUKE arm (DEKA) was used in place of the virtual prosthesis for some of P3’s trials.

During functional tasks, P3 performed a self-pace box and blocks task using a three DOF Kalman filter, trained with signals from the median RPNI, ulnar RPNI, FDPI, extensor pollicis longus, and

extensor digitorum communis. P4 sequentially performed a trio of SHAP abstract object tasks (light spherical, lateral, and power objects). Her two DOF Kalman filter was trained using the median RPNI, ulnar RPNI, and FDPI to control key pinch and power grip on the i-limb Quantum (Össur).

Simulated trajectories were generated by inputting EMG recorded during the functional tasks into Kalman filters trained only on residual muscle signals (FDPI, FPL, EDC, and EPL for P3, and FDPI and FPL for P4). The average Euclidean distance, normalized to the maximum range of motion, was calculated to measure the difference between the real-time and simulated trajectories. As an example for P3's two DOF thumb, the Euclidean dimensional space is 2 (dim = 2). The simulated trajectory, $\mathbf{s} = (s_1, s_2)$, represents a vector with Cartesian coordinates of the simulated thumb position in two-dimensional space. The original trajectory, $\mathbf{t} = (t_1, t_2)$, represents the original thumb position. In this plane, the Euclidean distance (d) from \mathbf{s} to \mathbf{t} is given by

$$d(\mathbf{s}, \mathbf{t}) = \sqrt{\sum_{i=1}^{\text{dim}} (s_i - t_i)^2}$$

The distance was then normalized to the maximum range of motion allowed by the virtual hand, which is the percentage difference between the simulated and original positions. This step was repeated on 16 and 33 samples of simulated and original thumb positions for P3 and P4, respectively, and the average was calculated across all samples. The Wilcoxon rank sum test was used to compare the difference between the simulated and original thumb trajectories.

To compare the two DOF thumb performance with surface electrodes, ultrasound was used to locate the RPNI in P4, and gelled surface electrodes (2-cm diameter) (Biopac Systems Inc.) were placed within a 4- to 6-cm radius above the RPNI location. Two electrodes were needed to create a bipolar recording. Since the two ulnar RPNI in P4 were separated by 1 cm, one pair of surface electrodes was used to record from both ulnar RPNI. Surface electrodes were also placed to capture the extensor pollicis longus and extensor digitorum communis signals.

For the discrete task training phase, P3 and P4 were cued a specific posture and asked to volitionally mirror the posture with their phantom limb. EMG data from only the RPNI were used to train a naïve Bayes classifier. During the decoding phase, the cue hand would instruct P3 and P4 to perform a specific posture, and they had to match it using a separate virtual hand (Fig. 4). The accuracy of the classifier was quantified by the number of correct predictions, whereas the speed of the classifier was measured by calculating the time between the EMG onset and the first correct predicted output from the classifier (Δt or movement selection time).

The discrete task training phase used the neural signal processor to record EMG signals, which were sent to the real-time computer where the MAV feature was calculated and saved in MATLAB. A separate computer smoothed the stored MAV feature in 50-ms bins for P4, and a sliding 50-ms window was updated every 10 ms for P3. A naïve Bayes classifier was then trained, and the matrix parameters were uploaded to the real-time computer. For the finger postures in Fig. 4, the classifier was trained with RPNI only signals, whereas the classifier for grasping postures in Fig. S3 was trained with RPNI and residual muscle signals (extensor pollicis longus, extensor digitorum communis, flexor pollicis longus, flexor digitorum profundus, and flexor carpi radialis). During the decoding phase, the participants held the cued

posture in the decoded hand for 1 s to successfully complete the trial. For P4, the online classifier outputted its prediction to the virtual prosthesis every 50 ms. For P3, the online classifier issued a prediction every 10 ms and was required to make five consecutive predictions before outputting the prediction to the virtual prosthesis.

Statistical analysis

Ultrasound videos, EMG, and finger position data were recorded and processed offline, and all statistical analysis was performed using MATLAB R2018a (MathWorks). Statistical comparisons were made using the Wilcoxon rank sum test at a significance level of $\alpha = 0.05$. All shaded traces indicate means ± 1 SD.

SUPPLEMENTARY MATERIALS

stm.sciencemag.org/cgi/content/full/12/533/eaay2857/DC1

Fig. S1. Electrode implantation for P3 and P4.

Fig. S2. P3 and P4's RPNI sonograms, motor map, and electrophysiology.

Fig. S3. Real-time classification of grasping hand postures.

Fig. S4. Original and simulated decodes during functional tasks.

Table S1. Details of a subset of muscles missing in each participant and their function.

Table S2. Quantitative analysis of ultrasound videos for P1.

Table S3. Calculated movement selection times for several postures between P3 and P4.

Table S4. Summary of observed RPNI grafts and the electrode type used to record EMG.

Movie S1. Ultrasound video capturing P1's median RPNI.

Movie S2. Ultrasound video capturing P1's ulnar RPNI.

Movie S3. Ultrasound video capturing two RPNI from P2.

Movie S4. P3's real-time discrete control of finger postures.

Movie S5. P4's real-time discrete control of finger postures.

Movie S6. P3 and P4's real-time discrete control of grasping postures.

Movie S7. P3's real-time continuous one DOF control up to 300 days.

Movie S8. P4's real-time continuous one DOF control up to 97 days.

Movie S9. P3 and P4's real-time continuous two DOF thumb control.

Movie S10. P4's real-time continuous two DOF thumb control using surface EMG.

Movie S11. P3's real-time continuous two DOF thumb using the LUKE arm.

Movie S12. P3 and P4's real-time continuous control during functional tasks.

[View/request a protocol for this paper from Bio-protocol.](#)

REFERENCES AND NOTES

1. T. A. Kung, R. A. Bueno, G. K. Alkhalefah, N. B. Langhals, M. G. Urbanchek, P. S. Cederna, Innovations in prosthetic interfaces for the upper extremity. *Plast. Reconstr. Surg.* **132**, 1515–1523 (2013).
2. X. Navarro, T. B. Krueger, N. Lago, S. Micera, T. Stieglitz, P. Dario, A critical review of interfaces with the peripheral nervous system for the control of neuroprostheses and hybrid bionic systems. *J. Peripher. Nerv. Syst.* **10**, 229–258 (2005).
3. T. S. Davis, H. A. C. Wark, D. T. Hutchinson, D. J. Warren, K. O'Neill, T. Scheinblum, G. A. Clark, R. A. Norman, B. Greger, Restoring motor control and sensory feedback in people with upper extremity amputations using arrays of 96 microelectrodes implanted in the median and ulnar nerves. *J. Neural Eng.* **13**, 036001 (2016).
4. S. Wendelken, D. M. Page, T. Davis, H. A. C. Wark, D. T. Kluger, C. Duncan, D. J. Warren, D. T. Hutchinson, G. A. Clark, Restoration of motor control and proprioceptive and cutaneous sensation in humans with prior upper-limb amputation via multiple Utah Slanted Electrode Arrays (USEAs) implanted in residual peripheral arm nerves. *J. Neuroeng. Rehabil.* **14**, 121 (2017).
5. J. A. George, D. T. Kluger, T. S. Davis, S. M. Wendelken, E. V. Okorokova, Q. He, C. C. Duncan, D. T. Hutchinson, Z. C. Thumser, D. T. Beckler, P. D. Marasco, S. J. Bensmaia, G. A. Clark, Biomimetic sensory feedback through peripheral nerve stimulation improves dexterous use of a bionic hand. *Sci. Robot.* **4**, eaax2352 (2019).
6. S. Raspopovic, M. Capogrosso, F. M. Petrini, M. Bonizzato, J. Rigosa, G. Di Pino, J. Carpaneto, M. Controzzi, T. Boretius, E. Fernandez, G. Granata, C. M. Oddo, L. Citi, A. L. Ciancio, C. Cipriani, M. C. Carrozza, W. Jensen, E. Guglielmelli, T. Stieglitz, P. M. Rossini, S. Micera, Restoring natural sensory feedback in real-time bidirectional hand prostheses. *Sci. Transl. Med.* **6**, 222ra19 (2014).
7. K. Horch, S. Meek, T. G. Taylor, D. T. Hutchinson, Object discrimination with an artificial hand using electrical stimulation of peripheral tactile and proprioceptive pathways with intrafascicular electrodes. *IEEE Trans. Neural Syst. Rehabil. Eng.* **19**, 483–489 (2011).
8. D. W. Tan, M. A. Schieber, M. W. Keith, J. R. Anderson, J. Tyler, D. J. Tyler, A neural interface provides long-term stable natural touch perception. *Sci. Transl. Med.* **6**, 257ra138 (2014).

9. Y. M. Dweiri, T. E. Eggers, L. E. Gonzalez-Reyes, J. Drain, G. A. McCallum, D. M. Durand, Stable detection of movement intent from peripheral nerves: Chronic study in dogs. *Proc. IEEE* **105**, 50–65 (2017).
10. P. Zhou, M. M. Lowery, K. B. Englehart, H. Huang, G. Li, L. Hargrove, J. P. A. Dewald, T. A. Kuiken, Decoding a new neural-machine interface for control of artificial limbs. *J. Neurophysiol.* **98**, 2974–2982 (2007).
11. J. E. Cheesborough, L. H. Smith, T. A. Kuiken, G. A. Dumanian, Targeted muscle reinnervation and advanced prosthetic arms. *Semin. Plast. Surg.* **29**, 62–72 (2015).
12. M. G. Urbanchek, Z. Baghmanli, J. D. Moon, K. B. Sugg, N. B. Langhals, P. S. Cederna, Quantification of regenerative peripheral nerve interface signal transmission. *Plast. Reconstr. Surg.* **130**, 55–56 (2012).
13. M. G. Urbanchek, T. A. Kung, C. M. Frost, D. C. Martin, L. M. Larkin, A. Wollstein, P. S. Cederna, Development of a regenerative peripheral nerve interface for control of a neuroprosthetic limb. *Biomed. Res. Int.* **2016**, 1–8 (2016).
14. P. P. Vu, Z. T. Irwin, A. J. Bullard, S. W. Ambani, I. C. Sando, M. G. Urbanchek, P. S. Cederna, C. A. Chestek, Closed-loop continuous hand control via chronic recording of regenerative peripheral nerve interfaces. *IEEE Trans. Neural Syst. Rehabil. Eng.* **26**, 515–526 (2018).
15. Z. T. Irwin, K. E. Schroeder, P. P. Vu, D. M. Tat, A. J. Bullard, S. L. Woo, I. C. Sando, M. G. Urbanchek, P. S. Cederna, C. A. Chestek, Chronic recording of hand prosthesis control signals via a regenerative peripheral nerve interface in a rhesus macaque. *J. Neural Eng.* **13**, 046007 (2016).
16. D. C. Ursu, M. G. Urbanchek, A. Nedic, P. S. Cederna, R. B. Gillespie, In vivo characterization of regenerative peripheral nerve interface function. *J. Neural Eng.* **13**, 026012 (2016).
17. T. A. Kung, N. B. Langhals, D. C. Martin, P. J. Johnson, P. S. Cederna, M. G. Urbanchek, Regenerative peripheral nerve interface viability and signal transduction with an implanted electrode. *Plast. Reconstr. Surg.* **133**, 1380–1394 (2014).
18. C. A. Kubiak, S. W. P. Kemp, P. S. Cederna, Regenerative peripheral nerve interface for management of postamputation neuroma. *JAMA Surg.* **153**, 681–682 (2018).
19. C. A. Kubiak, S. W. P. Kemp, P. S. Cederna, T. A. Kung, Prophylactic regenerative peripheral nerve interfaces to prevent postamputation pain. *Plast. Reconstr. Surg.* **144**, 421e–430e (2019).
20. S. L. Woo, T. A. Kung, D. L. Brown, J. A. Leonard, B. M. Kelly, P. S. Cederna, Regenerative peripheral nerve interfaces for the treatment of postamputation neuroma pain: A pilot study. *Plast. Reconstr. Surg. Glob. Open* **4**, e1038 (2016).
21. M. Sahin, M. A. Haxhiu, D. M. Durand, I. A. Dreshaj, Spiral nerve cuff electrode for recordings of respiratory output. *J. Appl. Physiol.* **83**, 317–322 (1997).
22. J. J. Struijk, M. Thomsen, J. O. Larsen, T. Sinkjaer, Cuff electrodes for long-term recording of natural sensory information. *IEEE Eng. Med. Biol. Mag.* **18**, 91–98 (1999).
23. W. D. Memberg, K. H. Polasek, R. L. Hart, A. M. Bryden, K. L. Kilgore, G. A. Nemunaitis, H. A. Hoyen, M. W. Keith, R. F. Kirsch, Implanted neuroprosthesis for restoring arm and hand function in people with high level tetraplegia. *Arch. Phys. Med. Rehabil.* **95**, 1201–1211.e1 (2014).
24. A. B. Ajiboye, R. F. Weir, A heuristic fuzzy logic approach to EMG pattern recognition for multifunctional prosthesis control. *IEEE Trans. Neural Syst. Rehabil. Eng.* **13**, 280–291 (2005).
25. C. Cipriani, C. Antfolk, M. Controzzi, G. Lundborg, B. Rosen, M. C. Carrozza, F. Sebelius, Online myoelectric control of a dexterous hand prosthesis by transradial amputees. *IEEE Trans. Neural Syst. Rehabil. Eng.* **19**, 260–270 (2011).
26. N. Jiang, H. Rehbaum, I. Vujaklija, B. Graumann, D. Farina, Intuitive, online, simultaneous, and proportional myoelectric control over two degrees-of-freedom in upper limb amputees. *IEEE Trans. Neural Syst. Rehabil. Eng.* **22**, 501–510 (2014).
27. G. Li, A. E. Schultz, T. A. Kuiken, Quantifying pattern recognition—Based myoelectric control of multifunctional transradial prostheses. *IEEE Trans. Neural Syst. Rehabil. Eng.* **18**, 185–192 (2010).
28. L. H. Smith, T. A. Kuiken, L. J. Hargrove, Use of probabilistic weights to enhance linear regression myoelectric control. *J. Neural Eng.* **12**, 066030 (2015).
29. T. A. Kuiken, G. Li, B. A. Lock, R. D. Lipschutz, L. A. Miller, K. A. Stubblefield, K. B. Englehart, Targeted muscle reinnervation for real-time myoelectric control of multifunction artificial arms. *JAMA* **301**, 619–628 (2009).
30. M. Sartori, G. Durandau, S. Došen, D. Farina, Robust simultaneous myoelectric control of multiple degrees of freedom in wrist-hand prostheses by real-time neuromusculoskeletal modeling. *J. Neural Eng.* **15**, 066026 (2018).
31. A. Ameri, E. N. Kamavuako, E. J. Scheme, K. B. Englehart, P. A. Parker, Support vector regression for improved real-time, simultaneous myoelectric control. *IEEE Trans. Neural Syst. Rehabil. Eng.* **22**, 1198–1209 (2014).
32. F. V. G. Tenore, A. Ramos, A. Fahmy, S. Acharya, R. Etienne-Cummings, N. V. Thakor, Decoding of individuated finger movements using surface electromyography. *IEEE Trans. Biomed. Eng.* **56**, 1427–1434 (2009).
33. M. D. Twardowski, S. H. Roy, Z. Li, P. Contessa, G. De Luca, J. C. Kline, Motor unit drive: A neural interface for real-time upper limb prosthetic control. *J. Neural Eng.* **16**, 016012 (2018).
34. S. Muceli, D. Farina, Simultaneous and proportional estimation of hand kinematics from emg during mirrored movements at multiple degrees-of-freedom. *IEEE Trans. Neural Syst. Rehabil. Eng.* **20**, 371–378 (2012).
35. B. Hudgins, P. Parker, R. N. Scott, A new strategy for multifunction myoelectric control. *IEEE Trans. Biomed. Eng.* **40**, 82–94 (1993).
36. L. J. Hargrove, L. A. Miller, K. Turner, T. A. Kuiken, Myoelectric pattern recognition outperforms direct control for transhumeral amputees with targeted muscle reinnervation: A randomized clinical trial. *Sci. Rep.* **7**, 13840 (2017).
37. J. M. Souza, J. E. Cheesborough, J. H. Ko, M. S. Cho, T. A. Kuiken, G. A. Dumanian, Targeted muscle reinnervation: A novel approach to postamputation neuroma pain. *Clin. Orthop. Relat. Res.* **472**, 2984–2990 (2014).
38. G. A. Dumanian, B. K. Potter, L. M. Mioton, J. H. Ko, J. E. Cheesborough, J. M. Souza, W. J. Ertl, S. M. Tintle, G. P. Nanos, I. L. Valerio, T. A. Kuiken, A. V. Apkarian, K. Porter, S. W. Jordan, Targeted muscle reinnervation treats neuroma and phantom pain in major limb amputees: A randomized clinical trial. *Ann. Surg.* **270**, 238 (2019).
39. E. Todorov, T. Erez, Y. Tassa, Mujoco: A Physics engine for model-based control, in 2012 IEEE/RSJ International Conference on Intelligent Robots and Systems (2012), pp. 5026–5033.

Funding: This work was supported by the Defense Advanced Research Projects Agency (DARPA) Biological Technologies Office (BTO) Hand Proprioception and Touch Interfaces (HAPTIX) program through the DARPA Contracts Management Office grant/contract no. N66001-16-1-4006 and by the National Institute Of Neurological Disorders And Stroke of the National Institutes of Health under Award Number R01NS105132 to C.A.C. P.P.V. and C.S.N. were supported by the National Science Foundation Graduate Research Fellowship Program under Award Number DGE 1256260. The opinions expressed in this article are the authors' own and do not reflect the view of the Department of Defense, National Institutes of Health, or the National Science Foundation. **Author contributions:** P.P.V., Z.T.I., C.A.C., and P.S.C. designed the study. P.P.V., A.K.V., and Z.T.I. completed the data gathering and development of analysis techniques with all authors contributing to the interpretation of results. P.T.H., D.R.L., and A.T.L. operated the ultrasound machine to locate RPNNs and residual muscles for acute fine wire implantation. P.S.C. developed and did the surgical implantation procedures. P.P.V., Z.T.I., A.K.V., and C.S.N. developed the software for the real-time experiments. P.P.V., T.A.K., S.W.P.K., A.J.D., C.A.C., D.H.G., R.B.G., and P.S.C. wrote the report. All authors provided critical review and approval of the report. **Competing interests:** The authors declare that they have no competing interests. The University of Michigan holds a patent related to this work, publication number US10314725B2: Method for amplifying signals from individual nerve fascicles. **Data and materials availability:** All data associated with this study are present in the paper or the Supplementary Materials.

Submitted 5 June 2019
Resubmitted 28 August 2019
Accepted 27 December 2019
Published 4 March 2020
10.1126/scitranslmed.aay2857

Citation: P. P. Vu, A. K. Vaskov, Z. T. Irwin, P. T. Henning, D. R. Lueders, A. T. Laidlaw, A. J. Davis, C. S. Nu, D. H. Gates, R. B. Gillespie, S. W. P. Kemp, T. A. Kung, C. A. Chestek, P. S. Cederna, A regenerative peripheral nerve interface allows real-time control of an artificial hand in upper limb amputees. *Sci. Transl. Med.* **12**, eaay2857 (2020).

Science Translational Medicine

A regenerative peripheral nerve interface allows real-time control of an artificial hand in upper limb amputees

Philip P. Vu, Alex K. Vaskov, Zachary T. Irwin, Phillip T. Henning, Daniel R. Lueders, Ann T. Laidlaw, Alicia J. Davis, Chrono S. Nu, Deanna H. Gates, R. Brent Gillespie, Stephen W. P. Kemp, Theodore A. Kung, Cynthia A. Chestek and Paul S. Cederna

Sci Transl Med **12**, eaay2857.
DOI: 10.1126/scitranslmed.aay2857

Hand(some) prosthetic technology

Neuroprosthetic devices providing tactile feedback sensation have been recently developed. Electrodes stimulating peripheral nerves have been shown to provide patients with the sense of touch and pressure when using upper limb prosthesis. Moreover, targeted muscle innervation can provide prosthesis control. However, the number of independent movements is still limited. Now, Vu *et al.* showed that regenerative peripheral nerve interfaces (RNPIs) implanted in upper limb amputees allowed the control of finger movements using hand prosthesis for almost a year without the need for adjustments. The results suggest that RNPIs could provide a stable and improved upper limb prosthesis control.

ARTICLE TOOLS

<http://stm.sciencemag.org/content/12/533/eaay2857>

SUPPLEMENTARY MATERIALS

<http://stm.sciencemag.org/content/suppl/2020/03/02/12.533.eaay2857.DC1>

RELATED CONTENT

<http://stm.sciencemag.org/content/scitransmed/10/432/eaao6990.full>
<http://stm.sciencemag.org/content/scitransmed/6/222/222ra19.full>
<http://stm.sciencemag.org/content/scitransmed/11/512/eaav8939.full>
<http://stm.sciencemag.org/content/scitransmed/8/362/362ra142.full>

REFERENCES

This article cites 38 articles, 2 of which you can access for free
<http://stm.sciencemag.org/content/12/533/eaay2857#BIBL>

PERMISSIONS

<http://www.sciencemag.org/help/reprints-and-permissions>

Use of this article is subject to the [Terms of Service](#)

Science Translational Medicine (ISSN 1946-6242) is published by the American Association for the Advancement of Science, 1200 New York Avenue NW, Washington, DC 20005. The title *Science Translational Medicine* is a registered trademark of AAAS.

Copyright © 2020 The Authors, some rights reserved; exclusive licensee American Association for the Advancement of Science. No claim to original U.S. Government Works